nature geoscience

ARTICLES

https://doi.org/10.1038/s41561-018-0243-0

O_2 solubility in Martian near-surface environments and implications for aerobic life

Vlada Stamenković[1,2*], Lewis M. Ward[2,3], Michael Mischna[1] and Woodward W. Fischer[2]

Due to the scarcity of O_2 in the modern Martian atmosphere, Mars has been assumed to be incapable of producing environments with sufficiently large concentrations of O_2 to support aerobic respiration. Here, we present a thermodynamic framework for the solubility of O_2 in brines under Martian near-surface conditions. We find that modern Mars can support liquid environments with dissolved O_2 values ranging from ~2.5×10^{-6} mol m^{-3} to 2 mol m^{-3} across the planet, with particularly high concentrations in polar regions because of lower temperatures at higher latitudes promoting O_2 entry into brines. General circulation model simulations show that O_2 concentrations in near-surface environments vary both spatially and with time—the latter associated with secular changes in obliquity, or axial tilt. Even at the limits of the uncertainties, our findings suggest that there can be near-surface environments on Mars with sufficient O_2 available for aerobic microbes to breathe. Our findings may help to explain the formation of highly oxidized phases in Martian rocks observed with Mars rovers, and imply that opportunities for aerobic life may exist on modern Mars and on other planetary bodies with sources of O_2 independent of photosynthesis.

Aerobic respiration is the most widespread and energetically favourable metabolism on Earth; it enabled complex multicellularity[1]. The history of O_2 and aerobic respiration on Earth is tied to that of photosynthesis, resulting today in ~21 vol% O_2 in a ~1 bar atmosphere[2]. In contrast, modern Mars has a thin, ~6.1 mbar, atmosphere with only trace amounts of O_2 produced from the photodissociation of CO_2 (ref. [3]). Molecular oxygen has been measured in situ by rovers, remotely by orbiters and from Earth-based observatories[4–7]. The data reveal a nearly constant volume mixing ratio of O_2 of $VMR_{O_2} \approx 0.145\%$ (ref.[4]).

Little attention has been given to the role of O_2 on Mars, due to its scarcity[3–7]; however, geochemical evidence from Martian meteorites[8] and manganese-rich rocks[9,10] points to highly oxidizing aqueous environments on Mars in its past, implying that O_2 played a role in the chemical weathering of the Martian crust[11].

Aqueous environments, in the form of brines, can exist today at, and especially below, the surface[12–14] despite the thin atmosphere and overall cold climate. Recent evidence demonstrates hydrated magnesium (Mg) and calcium (Ca) perchlorate salts at various locations on the Martian surface and shallow subsurface[12–15], which indicate the existence of $Mg(ClO_4)_2$-$Ca(ClO_4)_2$-H_2O brines, and which could, in some cases, be associated with flow structures such as the modern recurring slope lineae[12,13]. Ca- and Mg-perchlorate brines exhibit a much lower freezing point than pure water, by as much as 60–80 K (refs [16,17]), and at their eutectic composition, they effectively supercool down to 140–150 K before transitioning into a glass, even when mixed with Martian regolith simulant[16]. Calculations[18] and experiments[16] using brines containing Martian soil simulants with perchlorates (for example, an analogue of the Mars Phoenix landing site soil[18]) show that dissolved perchlorate concentrations can readily reach eutectic concentrations during freezing.

Meanwhile, whereas aerobic microbial life and simple animals need O_2 dissolved in liquids in sufficiently large concentrations to survive, recent experiments, observations and calculations have lowered the required limits of concentrations of dissolved O_2 for aerobic respiration to ~10^{-6} mol m^{-3} in microorganisms[19,20] and to ~2×10^{-3} mol m^{-3} in sponges[21].

The availability of O_2 in the Martian atmosphere, geological observations of oxidative weathering, the potential presence of cold liquid brines on, or beneath, the surface and low limits of dissolved O_2 concentrations needed for life raise the question of whether or not Mars could host liquid environments that contain sufficient amounts of dissolved O_2 to be capable of supporting aerobic metabolisms, and how such aerobic environments change with location on Mars, today and on timescales of obliquity change[22].

To address these questions, first, we develop a comprehensive thermodynamic framework applicable to Martian conditions that calculates the solubility of O_2 in liquid brines composed of water and salts, including perchlorates ($Ca(ClO_4)_2$, $Mg(ClO_4)_2$, $NaClO_4$), chlorides ($MgCl_2$, NaCl) and sulfates ($MgSO_4$). The supply of O_2 for our calculation is the atmosphere, and hence, our approach is valid for the surface and shallow subsurface ('near surface') only, where brines are assumed to communicate with the atmosphere.

Second, we couple this solubility framework to a Mars general circulation model (GCM)[23,24] to compute the solubility of O_2 as a function of annually averaged values of pressure and temperature varying with location on Mars today (for an obliquity of ~25°). Using annual average climate values precludes the specifics of diurnal and seasonal variations of these aerobic environments, but gives a concise first look into the regions that are most or least likely to sustain high O_2 solubilities.

Third, we examine how the distribution of aerobic environments evolved over the past 20 Myr and how it may change in the next 10 Myr. To achieve this, we (1) extend the modern-day Mars climate model[23,24] using different values of obliquity (5°, 10°, 15°, 17°, 20°, 40°, 60°, 90°) to obtain annually averaged climate maps for each obliquity and (2) use calculations of Mars's obliquity changes over the past ~20 Myr and the next ~10 Myr (ref. [22]) to identify epochs with different axial tilts.

The fundamental challenge is to describe gas dissolution processes in brines for a wide range of temperatures, including those

[1]Jet Propulsion Laboratory, California Institute of Technology, Pasadena, CA, USA. [2]Division of Geological and Planetary Sciences, California Institute of Technology, Pasadena, CA, USA. [3]Harvard University, Cambridge, MA, USA. *e-mail: Vlada.Stamenkovic@jpl.nasa.gov

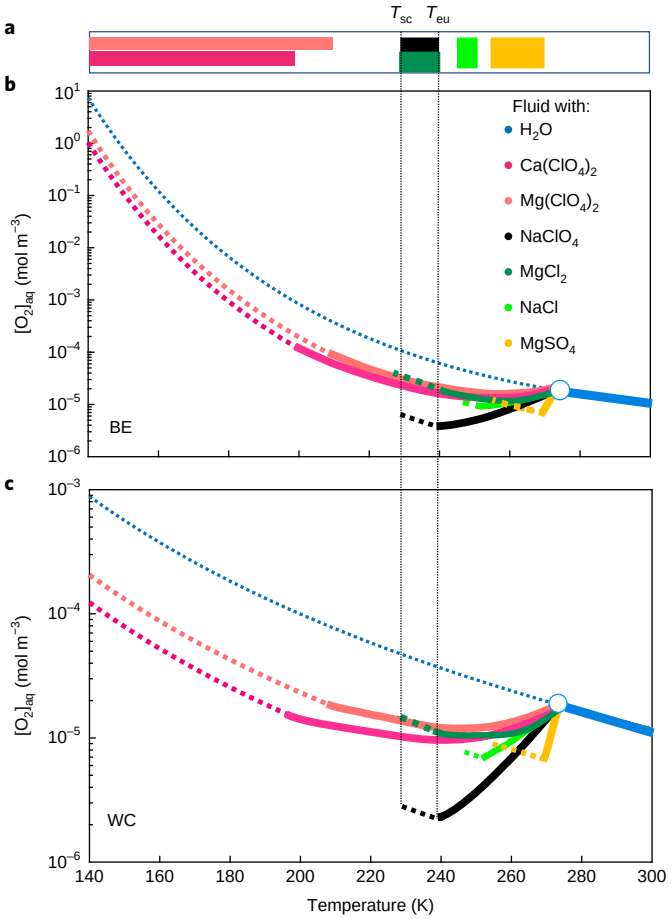

Fig. 1 | Solubility of O_2 in liquids on modern Mars as a function of temperature for 6.1 mbar. a, Feasible supercooling domain between eutectic temperature, T_{eu}, and maximum supercooling temperature, T_{sc} (refs [16,17,26]) (see Supplementary Table 3). **b**,**c**, Using the minimum salt concentration needed to enable a liquid brine[16,17,26], we plot the change of dissolved O_2 concentrations ($[O_2]_{aq}$, where 'aq' indicates aqueous solution) with temperature, using modern Mars temperatures (~140–300 K) and an average surface pressure of 6.1 mbar; BE, best estimate (**b**); WC, conservative worst case (**c**). Each fluid is colour coded based on the salt that it contains (see key in **b**); solid line for temperatures above the eutectic temperature and dashed line between the eutectic and maximum supercooling temperature. For pure water (blue), we plot for completeness the theoretical solubility below 273 K as a dotted line.

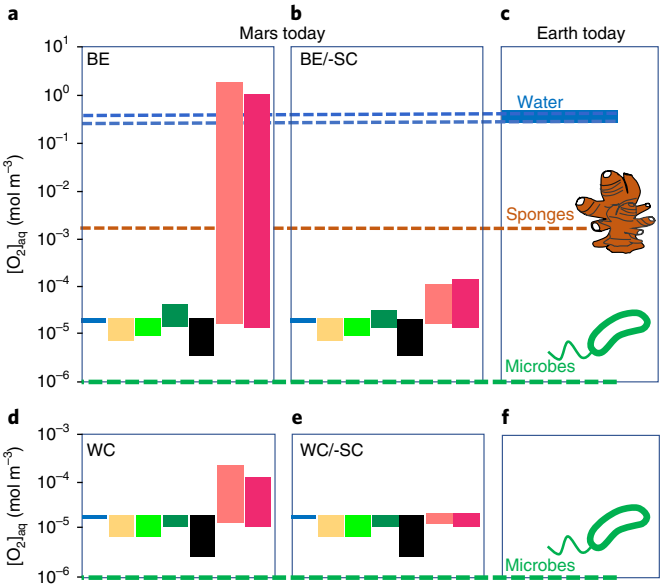

Fig. 2 | O_2 solubilities in liquids on modern Mars for 6.1 mbar and 140–300 K compared with Earth today. a–f, Using the O_2 solubility for $T = 140$–300 K and 6.1 mbar from Fig. 1 (colour code for brines same as in Fig. 1), we obtain the range of possible O_2 solubilities on modern Mars for the BE (**a**) and the WC (**d**) with supercooling, and without supercooling (BE/-SC (**b**) and WC/-SC (**e**)), in comparison with dissolved O_2 levels required for aerobic respiration by microbes[19,20] (green dashed lines) and simple animals such as sponges[21] (brown dashed line) and found in pure water on modern Earth ($T \approx 273$–300 K, blue dashed lines) (**c**,**f**). Before the Great Oxygenation Event, the solubility of O_2 was probably ~10^{-13}–10^{-6} mol m^{-3}.

below the freezing point of water. To achieve this, first, we compute how the solubility of O_2 would change as a function of temperature in supercooled water. The critical uncertainty for this computation involves the specific heat of dissolved O_2 in supercooled water. To address this uncertainty, we derive a conservative estimate by assuming a constant value for the specific heat of dissolved O_2 below 273 K; we refer to this as our best estimate. The best estimate agrees to within a few percent with available data. Second, we test plausible alternatives for the behaviour of the specific heat of supercooled water[25] and brines[25,26] (this leads to a negligible difference from our best estimate). Third, we derive a thermodynamic lower limit, which we refer to as the worst case, for the solubility of O_2 (see Methods).

The presence of dissolved cations and anions (for $Ca(ClO_4)_2$, Ca^{2+} and ClO_4^-) reduces the solubility of O_2 in water[27]. To account for this 'salting out'[28] of O_2, we use the Pitzer model[29] to compute O_2–cation, O_2–anion and O_2–cation–anion electrostatic interactions. We also estimate the temperature dependence of the Pitzer coefficients (Supplementary Section 2.1.4), but find it to be negligible, in agreement with other Mars brine studies[30] and experimental data[31].

The O_2 solubility levels in brines on modern Mars

We examine the solubility of O_2 for various potential Martian brines as a function of Mars temperatures from 140 K to 300 K for an average Mars surface pressure of ~6.1 mbar, assuming, for each temperature, the critical minimum concentration of salt needed for the brine to remain liquid (Fig. 1b for our best estimate and Fig. 1c for the worst case). We then plot the levels of dissolved O_2 possible on modern Mars—with and without supercooling—in comparison with O_2 levels on modern Earth that are required by life or are found in pure water (Fig. 2).

Next to having very low eutectic temperatures[16,17], Mg- and Ca-perchlorate brines can exist as liquids in a supercooled state far below their eutectic temperature, as shown by experiments (~209 K and ~198 K, respectively)[16,] to ~140–150 K under modern Martian conditions (Fig. 1a and Supplementary Information). Therefore, O_2 solubilities for Mg- and Ca-perchlorate brines can increase substantially by up to five orders of magnitude from 273 K to 140 K for our best estimate, with solubility values for 6.1 mbar of 10^{-5}–10^{0} mol m^{-3} (Figs. 1b and 2a). In comparison with our best estimate, the O_2 solubilities for the worst case at 140 K for Ca- and Mg-perchlorates are reduced, but the O_2 solubility still increases by more than one order of magnitude from 273 K to 140 K, with values as high as 2×10^{-4} mol m^{-3} for 6.1 mbar (Figs. 1c and 2d).

Without supercooling, O_2 solubilities in near-surface Ca- and Mg-perchlorate brines are still roughly 1–2 orders of magnitude above 10^{-6} mol m^{-3} on modern Mars (Figs. 2b,e and 3).

Other brines that we study show higher eutectic temperatures and lower degrees of supercooling (Supplementary Table 3). If we

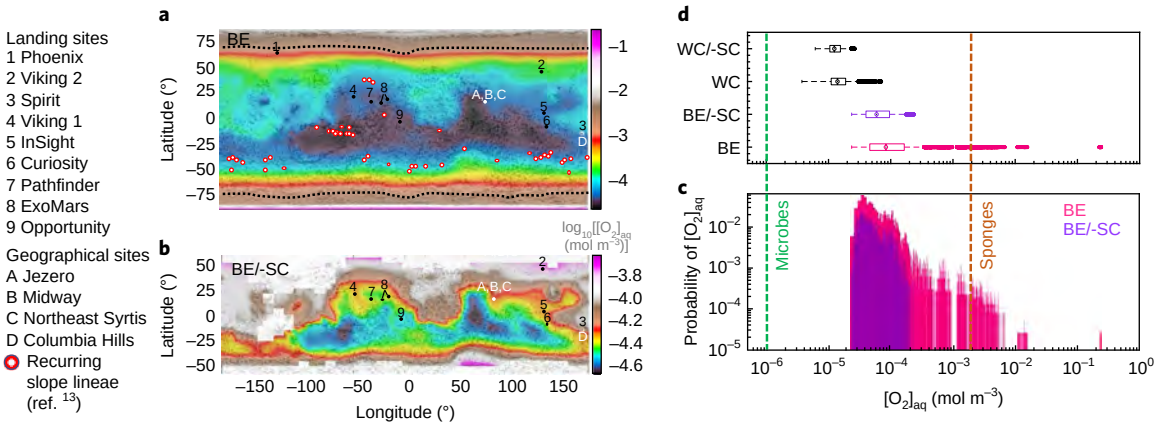

Fig. 3 | Spatial variation of O_2 solubility in Ca-perchlorate brines on modern Mars. a,**b**, Maps of $[O_2]_{aq}$ according to the best estimate for the annually averaged O_2 solubility $[O_2]_{aq}$ in Ca-perchlorate brines with supercooling (BE) (**a**) and without supercooling (BE/-SC) (**b**), under modern Martian conditions with a perennial south polar CO_2 cap. Without supercooling, mainly latitudes equatorward of ~50° favour liquid brines. In **a**, the black dashed lines mark poleward solubility values above the aerobic respiration limit for sponges. **c**,**d**, Histogram and boxplots of $[O_2]_{aq}$ values for Ca-perchlorate brines and BE with (red) and without (purple) supercooling, and biological breathing limits (dashed lines). In **d**, the central mark indicates the median, and the bottom (Q_1) and top (Q_3) edges of the box indicate the 25th and 75th percentiles, respectively. With IQR = $Q_3 - Q_1$, the whiskers extend to $Q_1 - 1.5$ IQR or above $Q_3 + 1.5$ IQR, and the outliers are plotted individually as dots. Comparable results for Mg-perchlorate.

assume these compositions, the results yield lower O_2 solubilities, with values around ~10^{-5} mol m^{-3} varying by up to one order of magnitude across modern Mars (Fig. 2).

As potential sources of uncertainty, we estimate a possible temperature dependence of the Pitzer coefficients by using a derivative of the apparent volume model[32], but find no considerable change. Also, we find the variability of the mixing ratio for O_2 to be too small to affect the conclusions (see Supplementary Information).

Spatial variation of O_2 solubility

The O_2 near-surface solubility is primarily controlled by temperature and secondarily by pressure—both of which vary substantially across Mars's surface. To assess spatial variation in dissolved O_2 concentrations, we connect the O_2 solubility calculations for Ca- and Mg-perchlorate brines with a climate model for modern Mars[23,24]. For each temperature, we compute the critical concentration of $Ca(ClO_4)_2$ or $Mg(ClO_4)_2$ needed for the brine to remain liquid, and then solve for the solubility of O_2 under scenarios with and without supercooling for the two solubility models (best estimate and worst case; see Fig. 3).

For our best estimate (including supercooling), the results display large gradients in O_2 solubility for Ca- and Mg-perchlorates across Mars, with polar regions having the greatest potential to harbour near-surface fluids at 2×10^{-1} mol m^{-3} of dissolved O_2, and the least O_2-rich environments in the tropical southern highlands at ~2.5×10^{-5} mol m^{-3} of dissolved O_2. The O_2 solubility of near-surface brines across Mars today could vary by five orders of magnitude (Fig. 3a). This trend results from lower temperatures at higher latitudes promoting O_2 entry into brines.

For our best estimate, but without supercooling, liquid perchlorate brines can occur primarily at equatorward latitudes below 50° and −50°, with differences in potential O_2 solubility of one order of magnitude, depending on the specific location (Fig. 3b).

Even for the worst case (with and without supercooling), values for the solubility of O_2 in Ca- and Mg-perchlorate near-surface brines are generally 1–2 orders of magnitude above 10^{-6} mol m^{-3} (Figs. 2d,e and 3d).

Obliquity-driven variations in O_2 solubility

We extend our results to examine how O_2 solubility in Ca- and Mg-perchlorate brines varies with climates at different obliquities, assuming the modern Mars atmospheric inventory. We find that for obliquities of less than ~10–15°, Mars experiences episodes of atmospheric collapse, where the condensable species in the atmosphere (mainly CO_2) form thick polar ice caps. Such events are rare in the interval we study[22] (Fig. 4b), and their potential effects on O_2 solubility are described in the Supplementary Information.

For the best estimate and worst case (with supercooling), the range of, the average and the maximum O_2 solubility can substantially decrease for higher obliquities (Fig. 4a), due to the minimum surface temperature being generally higher for an increasing obliquity (Supplementary Table 4).

We also examine the potential of the south polar cap fully sublimating at higher obliquities and roughly doubling the surface pressure. We find for our best estimate that the additional increase in surface temperatures of ~4 K from doubling the surface pressure (Supplementary Table 4) compensates for the increase in solubility due to the increased surface pressure; for the worst case, the results, shown in Fig. 4, remain also similar.

Integrating these results with obliquity variation through time[22], it is apparent that the past 5 Myr have supported particularly O_2-rich environments (Fig. 4c), while the preceding 15 Myr favoured average maximum O_2 solubility values in Mg- and Ca-perchlorate brines up to ~200 times lower than today. These results demonstrate the possibility of a substantial secular variation in the O_2 content of fluids such as Mg- and Ca-perchlorate brines in Mars's near-surface environments over its recent history.

Implications for aerobic life on Mars

We find that, on modern Mars—accounting for all uncertainties, for our best estimate and the worst case, both with and without supercooling and also for temperatures above 273 K where our solubility model has been validated—the solubility of O_2 in various fluids can exceed the level required for aerobic respiration of ~10^{-6} mol m^{-3} for microbes[19,20] by ~1–6 orders of magnitude (Figs. 2 and 3). In Ca- and Mg-perchlorate brines, O_2 solubilities can reach values comparable to the concentrations of O_2 in Earth's oceans today (Fig. 2a–c).

In comparison, the solubility of O_2 in seawater (assuming modern salinity and 293 K) on early Earth before the Great Oxygenation Event about 2.35 billion years ago[2] was probably ~10^{-13}–10^{-6} mol m^{-3}, on the basis of estimates of the partial pressure of O_2 (refs [33–35]). Therefore, the dissolved O_2 levels on early Earth were primarily

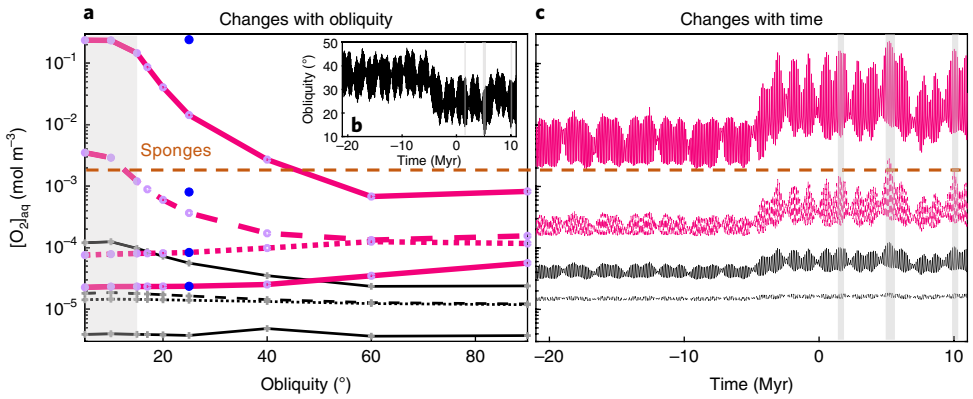

Fig. 4 | Evolution of aerobic environments on Mars due to obliquity change for Ca-perchlorate brines. a, With supercooling, BE (purple dots with red line) and WC (grey crosses with black line) for global maximum (top solid), minimum (bottom solid), average (dashed) and median (dotted) O_2 solubilities in Ca-perchlorate brines with varying obliquity (for a climate model without a perennial south polar CO_2 cap; blue dots are BE results (from top to bottom: maximum, average, median, minimum) for modern Mars with a perennial south polar CO_2 cap as in Fig. 3; for WC, there is no difference between south polar cap and no south polar cap cases). **b**, Predicted obliquity variation across time[22]. **c**, Using **a** and **b**, we plot global maximum (top) and average (bottom) $[O_2]_{aq}$ values for BE (red lines) and WC (black lines) across time for Ca-perchlorate brines. Dashed brown lines highlight the aerobic breathing limit for sponges and grey shaded boxes obliquities/times where we find atmospheric collapse. Comparable results for Mg-perchlorate.

below the minimum concentration of dissolved oxygen needed to support aerobic life. By comparison, modern Mars enables greater O_2 solubilities due to its much colder surface temperatures in relation to early Earth and a small but relevant amount of atmospheric O_2. Thus, in principle, Mars could offer a wide range of near-surface environments with enough dissolved O_2 for aerobic respiration like that seen in diverse groups of terrestrial microorganisms.

Moreover, for supercooled Ca- and Mg-perchlorate brines on Mars today, ~6.5% of the total Martian surface area could support far higher dissolved O_2 concentrations—enabling aerobic oases at dissolved O_2 concentrations higher than 2×10^{-3} mol m^{-3}, sufficient to sustain the respiration demands of more complex multicellular organisms such as sponges[21] (Figs. 2 and 3). Such aerobic oases are common today at latitudes poleward of about 67.5° and about −72.5° (Fig. 3a). These aerobic oases are feasible for low obliquities, but become unlikely for obliquities of more than ~45–50° (Fig. 4a). Such high-obliquity states were uncommon in the last 20 Myr (ref. [22]).

Other aerobic environments with intermediate O_2 solubilities of ~10^{-4}–10^{-3} mol m^{-3} can occur today closer to the equator in areas of lower topography, such as Hellas, Arabia Terra, Amazonis Planitia and Tempe Terra, with larger mean surface pressures (Fig. 3a).

The trends we show here are robust, as they can be tracked back to model-independent findings: (1) higher solubility for lower temperature and higher pressure, (2) temperature as the main control factor for solubility, (3) the poles being colder than the equator for modern Mars and (4) the poles generally warming at higher obliquities. Multicomponent brines containing more than one salt are a natural extension of our work, but binary saltwater mixtures, as studied in this work, suffice to exemplify the aerobic potential of near-surface Martian brines.

At the solubilities we find, O_2 could play a role in chemical weathering of Mars's crust[11,36] and may help to explain a range of surprising geochemical, geological and atmospheric observations, including the presence of highly oxidized phases in Martian rocks[9–11] and seasonal variability of methane at Gale crater[37].

Our study focused on near-surface environments. Recent results have indicated the potential existence of Ca- and Mg-perchlorate-rich subsurface brines at a temperature of ~205 K and a depth of 1.5 km (ref. [38]). Our results imply that the O_2 solubility in such a reservoir would be high, raising the possibility that they could be rich in O_2 if the supply either from intermittent communication with the atmosphere or from the radiolysis of water is sufficiently large.

We do not know whether or not Mars was ever host to life; recent efforts have focused profitably on the related question of habitability[39]. Our results can add O_2 solubility as an additional dimension to explore Martian habitability, where aerobic environments could act as resources for life (Supplementary Section 3).

On Earth, aerobic respiration appears to have followed in the evolutionary footsteps of oxygenic photosynthesis, reflecting the scarcity of O_2 on Earth before photosynthesis. However, by sourcing O_2 in a different way, Mars shows us this need not be the case, broadening our view of the opportunities for aerobes on other planetary bodies.

Online content

Any methods, additional references, Nature Research reporting summaries, source data, statements of data availability and associated accession codes are available at https://doi.org/10.1038/s41561-018-0243-0.

Received: 26 March 2018; Accepted: 11 September 2018;
Published online: 22 October 2018

References

1. Catling, D. C., Glein, C. R., Zahnle, K. J. & McKay, C. P. Why O_2 is required by complex life on habitable planets and the concept of planetary 'oxygenation time'. *Astrobiology* **5**, 415–438 (2005).
2. Fischer, W. W., Hemp, J. & Johnson, J. E. Evolution of oxygenic photosynthesis. *Annu. Rev. Earth Planet. Sci.* **44**, 647–683 (2016).
3. Nair, H., Allen, M., Anbar, A. D., Yung, Y. L. & Clancy, R. T. A photochemical model of the Martian atmosphere. *Icarus* **111**, 124–150 (1994).
4. Mahaffy, P. R. et al. Abundance and isotopic composition of gases in the Martian atmosphere from the Curiosity rover. *Science* **341**, 263–266 (2013).
5. Barker, E. S. Detection of molecular oxygen in the Martian atmosphere. *Nature* **238**, 447–448 (1972).
6. Owen, T. et al. The composition of the atmosphere at the surface of Mars. *J. Geophys. Res.* **82**, 4635–4639 (1977).
7. Hartogh, P. et al. Herschel/HIFI observations of Mars: fi st detection of O_2 at submillimeter wavelength and upper limits on HCl and H_2O_2. *Astron. Astrophys.* **521**, L49 (2010).
8. Shaheen, R., Niles, P. B., Chong, K., Corrigan, C. M. & Thie ens, M. H. Carbonate formation events in ALH84001 trace the evolution of the Martian atmosphere. *Proc. Natl Acad. Sci. USA* **112**, 336–341 (2015).
9. Lanza, N. L. et al. High manganese concentrations in rocks at Gale crater, Mars. *Geophys. Res. Lett.* **41**, 5755–5763 (2014).
10. Arvidson, R. E. et al. High concentrations of manganese and sulfur in deposits on Murray Ridge, Endeavour crater, Mars. *Am. Mineral.* **101**, 1389–1405 (2016).

11. Hurowitz, J. A. Redox stratifi ation of an ancient lake in Gale crater, Mars. *Science* **356**, eaah6849 (2017).
12. Ojha, L. et al. Spectral evidence for hydrated salts in recurring slope lineae on Mars. *Nat. Geosci.* **8**, 829–832 (2015).
13. Rummel, J. D. et al. A new analysis of Mars 'Special Regions': fi dings of the second MEPAG Special Regions Science Analysis Group (SR-SAG2). *Astrobiology* **14**, 887–968 (2014).
14. Kounaves, S. P. et al. Identifi ation of the perchlorate parent salts at the Phoenix Mars landing site and possible implications. *Icarus* **232**, 226–231 (2014).
15. Leshin, L. A. et al. Volatile, isotope, and organic analysis of Martian fi es with the Mars Curiosity rover. *Science* **341**, 1238937 (2013).
16. Toner, J. D., Catling, D. C. & Light, B. The formation of supercooled brines, viscous liquids, and low-temperature perchlorate glasses in aqueous solutions relevant to Mars. *Icarus* **233**, 36–47 (2014).
17. Pestova, O. N., Myund, L. A., Khripun, M. K. & Prigaro, A. V. Polythermal study of the systems $M(ClO_4)_2$-H_2O (M^{2+} = Mg^{2+}, Ca^{2+}, Sr^{2+}, Ba^{2+}). *Russ. J. Appl. Chem.* **78**, 409–413 (2005).
18. Marion, G. M., Catling, D. C., Zahnle, K. J. & Claire, M. W. Modeling aqueous perchlorate chemistries with applications to Mars. *Icarus* **207**, 675–685 (2010).
19. Zakem, E. J. & Follows, M. J. A theoretical basis for a nanomolar critical oxygen concentration. *Limnol. Oceanogr.* **62**, 795–805 (2017).
20. Stolper, D. A., Revsbech, N. P. & Canfi ld, D. E. Aerobic growth at nanomolar oxygen concentrations. *Proc. Natl Acad. Sci. USA* **107**, 18755–18760 (2010).
21. Mills, D. B. et al. Oxygen requirements of the earliest animals. *Proc. Natl Acad. Sci. USA* **111**, 4168–4172 (2014).
22. Laskar, J. et al. Long term evolution and chaotic diffusion of the insolation quantities of Mars. *Icarus* **170**, 343–364 (2004).
23. Richardson, M. I., Toigo, A. D. & Newman, C. E. PlanetWRF: a general purpose, local to global numerical model for planetary atmospheric and climate dynamics. *J. Geophys. Res.* **112**, E09001 (2007).
24. Toigo, A. D., Lee, C., Newman, C. E. & Richardson, M. I. The impact of resolution on the dynamics of the Martian global atmosphere: varying resolution studies with the MarsWRF GCM. *Icarus* **221**, 276–288 (2012).
25. Archer, D. G. & Carter, R. W. Thermodynamic properties of the NaCl + H_2O system. 4. Heat capacities of H_2O and NaCl(aq) in cold-stable and supercooled states. *J. Phys. Chem. B* **104**, 8563–8584 (2000).
26. Toner, J. D. & Catling, D. C. Water activities of $NaClO_4$, $Ca(ClO_4)_2$, and $Mg(ClO_4)_2$ brines from experimental heat capacities: water activity >0.6 below 200 K. *Geochim. Cosmochim. Acta* **181**, 164–174 (2016).
27. Clegg, S. L. & Brimblecombe, P. The solubility and activity coeffici t of oxygen in salt solutions and brines. *Geochim. Cosmochim. Acta* **54**, 3315–3328 (1990).
28. Konnik, E. I. Salting-out and salting-in of gaseous non-electrolytes in aqueous solutions of electrolytes. *Russ. Chem. Rev.* **46**, 577–588 (1977).
29. Pitzer, K. S. Theoretical considerations of solubility with emphasis on mixed aqueous electrolytes. *Pure Appl. Chem.* **58**, 1599–1610 (1989).
30. Toner, J. D., Catling, D. C. & Light, B. A revised Pitzer model for low-temperature soluble salt assemblages at the Phoenix site, Mars. *Geochim. Cosmochim. Acta* **166**, 327–343 (2015).
31. Silvester, L. F. & Pitzer, K. S. Thermodynamics of electrolytes. X. Enthalpy and the effect of temperature on the activity coeffici ts. *J. Solution Chem.* **7**, 327–337 (1978).
32. Tromans, D. Modeling oxygen solubility in water and electrolyte solutions. *Ind. Eng. Chem. Res.* **39**, 805–812 (2000).
33. Kasting, J. F., Liu, S. C. & Donahue, T. M. Oxygen levels in the prebiological atmosphere. *J. Geophys. Res.* **84**, 3097–3107 (1979).
34. Pavlov, A. A. & Kasting, J. F. Mass-independent fractionation of sulfur isotopes in Archean sediments: strong evidence for an anoxic Archean atmosphere. *Astrobiology* **2**, 27–41 (2002).
35. Lyons, T. W., Reinhard, C. T. & Planavsky, N. J. The rise of oxygen in Earth's early ocean and atmosphere. *Nature* **506**, 307–315 (2014).
36. Johnson, J. E., Gerpheide, A., Lamb, M. P. & Fischer, W. W. O_2 constraints from Paleoproterozoic detrital pyrite and uraninite. *Geol. Soc. Am. Bull.* **126**, 813–830 (2014).
37. Webster et al. Background levels of methane in Mars' atmosphere show strong seasonal variations. *Science* **360**, 1093–1096 (2018).
38. Orosei, et al. Radar evidence of subglacial liquid water on Mars. *Science* **361**, 1093–1096 (2018).
39. Grotzinger, J. P. & Milliken, R. E. in *Sedimentary Geology of Mars* SEPM Special Publication Vol. 102 (eds Grotzinger, J. P. & Milliken, R. E.) 1–48 (Society for Sedimentary Geology, Tulsa, 2012).

Acknowledgements

V.S. would like to dedicate this work in memory of A. S. Kubik who inspired so many to search for life on other worlds and brought so much life to this planet. V.S. thanks the Simons Foundation Collaboration on the Origins of Life for supporting this work (338555). A portion of this work was performed at the Jet Propulsion Laboratory, California Institute of Technology, under a contract with NASA. W.W.F. acknowledges support of the David and Lucile Packard Foundation and Simons Foundation Collaboration on the Origins of Life, and L.M.W. the support of a NASA Earth Space and Science Fellowship. Resources supporting this work were provided by the NASA High-End Computing (HEC) Program through the NASA Advanced Supercomputing (NAS) Division at Ames Research Center as well as the High-Performance Computing facilities of the Jet Propulsion Laboratory, Office of the Chief Information Officer.

Author contributions

V.S., L.M.W. and W.W.F. conceptualized this study. M.M. ran the GCM simulations for all obliquities. V.S. developed the solubility model for all brines, extended the idea to a three-dimensional and time-dependent (obliquity-driven) solubility framework, led the writing of the manuscript and prepared all figures and tables. All authors contributed to the writing of the manuscript.

Competing interests

The authors declare no competing interests.

Additional information

Supplementary information is available for this paper at https://doi.org/10.1038/s41561-018-0243-0.

Reprints and permissions information is available at www.nature.com/reprints.

Correspondence and requests for materials should be addressed to V.S.

Publisher's note: Springer Nature remains neutral with regard to jurisdictional claims in published maps and institutional affiliations.

Methods

Below, we summarize our methods—from solubility to GCM—needed to reproduce our results. We direct the reader to the Supplementary Information for the derivation of all used equations and details on any Methods subsection.

Solubility model. The solubility of O_2 is the number of dissolved O_2 molecules ($[\widetilde{O}_2]_{aq,X}$ in mol kg^{-1} and $[O_2]_{aq,X}$ in mol m^{-3}, where 'aq' indicates aqueous solution) in a brine consisting of m_X mol of salt X per kg of pure water in equilibrium with an atmosphere of pressure, P, surface temperature, T, and the volume mixing ratio, VMR_{O_2} ($VMR_{O_2} \times P$ corresponds to the total partial O_2 pressure in the atmosphere, p_{O_2}).

To compute $[\widetilde{O}_2]_{aq,X}$, we start with the solubility of O_2 in pure water, $[\widetilde{O}_2]_{aq,w}$:

$$[\widetilde{O}_2]_{aq,w}(T,P) = \frac{p_{O_2}}{P_{ref}} \exp\left(\frac{\tilde{\mu}_{g,O_2}(T) - \tilde{\mu}_{aq,w,O_2}(T)}{RT}\right) \quad (1)$$

where $\tilde{\mu}(T)$ is the chemical potential as a function of temperature at fixed reference pressure, P_{ref}, with $\tilde{\mu}_{g,O_2}(T)$ for O_2 in the gas phase and $\tilde{\mu}_{aq,w,O_2}(T)$ for O_2 dissolved in water, and R is the molar gas constant.

To compute $[\widetilde{O}_2]_{aq,w}$, we need to determine the difference in molar chemical potential, evaluated at P_{ref}, between O_2 dissolved in pure water and in the gas phase, $\Delta\tilde{G}(T) = \tilde{\mu}_{aq,w,O_2}(T) - \tilde{\mu}_{g,O_2}(T)$, as a function of temperature, in J mol^{-1}. The difference in chemical potential corresponds to the difference in molar Gibbs potential between O_2 in the gaseous and dissolved phases:

$$\tilde{\mu}(T) = \tilde{\mu}(T_{ref}) - S(T_{ref}) \times [T - T_{ref}] + \int_{T_{ref}}^{T} C_P(T')\,dT' - T\int_{T_{ref}}^{T} \frac{C_P(T')}{T'}\,dT' \quad (2)$$

To calculate $\tilde{\mu}(T)$ for O_2 either in the gas phase or in the dissolved phase, we need to know the values of their chemical potentials $\tilde{\mu}(T_{ref})$, in J mol^{-1}, and molar entropy $S(T_{ref})$, in J K^{-1} mol^{-1}, at a reference temperature, T_{ref} (both have been previously measured in experiments[40]), and the temperature dependence of the molar specific heat at constant pressure, $C_P(T)$, in J K^{-1} mol^{-1}. The parameters needed to solve equations (1) and (2) are listed in Supplementary Table 1 and can be found in the literature[40]. For the choice of the temperature dependence of the specific heat capacity at constant pressure of gaseous and dissolved O_2, see the section below, 'Specific heats and robustness of conclusions'.

After computing the solubility of O_2 in pure supercooled water, we need to quantify the electrostatic interactions between the water dipoles and the ions in solution, because these cause a reduction in apparent water volume that can be used to dissolve O_2 (refs [32,40,41]), and hence, the solubility of O_2 in a brine containing a salt, X, of molality m_X is reduced by a salting-out factor of $\gamma_{O_2}(X, m_X)$ compared with pure water:

$$[\widetilde{O}_2]_{aq,X}(T,P) = \frac{1}{\gamma_{O_2}(X, m_X)} [\widetilde{O}_2]_{aq,w}(T,P) \quad (3)$$

Experiments and theory have demonstrated that $\gamma_{O_2}(X, m_X)$ depends only weakly on temperature[27,31,42]. As shown in the Supplementary Information in detail, we use available data on various salts from 300 K to 240 K as well as theoretical calculations to demonstrate that for perchlorates too, we expect, from 298 K to 140 K, only a weak temperature-induced increase of $\gamma_{O_2}(X, m_X)$ by less than a factor of 3–10 (and probably less than a factor of 5).

The electrostatic interactions can be separated into first-order direct undisturbed interactions between the O_2 molecules and the dissolved cations, O_2–c, and anions, O_2–a, respectively. Such interactions are described with the Pitzer approach[29] through interaction coefficients, λ_{O_2-c} and λ_{O_2-a}, and the corresponding molalities for the cations, m_c, and anions, m_a, respectively. The secondary interaction between the triplet of cations, anions and O_2 molecules, λ_{O_2-c-a}, is normally negative[27,29] because secondary interactions generally weaken the electrostatic primary exchange of cations or anions with the O_2 molecule, which therefore decreases the salting-out factor and leads to an effective increase of the gas solubility. Setting $\lambda_{O_2-c-a} = 0$ marks, hence, a lower bound for the solubility. To make the salting-out factor a function of m_X, we use, for each ion (cation and anion), the mol(ion)/mol(salt) fractions, f_c and f_a. The parameters needed to solve equations (3) and (4) are in Supplementary Table 2 and can be taken from or computed with available data[27,28,43].

$$\begin{aligned}\gamma_{O_2}(X) &= \exp\left(\sum_c 2\lambda_{O_2-c} m_c + \sum_a 2\lambda_{O_2-a} m_a + \sum_c \sum_a \lambda_{O_2-c-a} m_c m_a\right) \\ &= \exp\left(2\sum_c \lambda_{O_2-c} f_c m_X + 2\sum_a \lambda_{O_2-a} f_a m_X \right. \\ &\quad \left. + \sum_a \sum_c \lambda_{O_2-c-a} f_a f_c m_X^2\right)\end{aligned} \quad (4)$$

We convert $[\widetilde{O}_2]_{aq,X}$ into $[O_2]_{aq,X}$ (which is used for Figs. 1–4) in equation 5 because it is the volume number density that is relevant to chemistry and respiration.

$$[O_2]_{aq,X}(T,P) = \rho_{brine}(T,P) \times [\widetilde{O}_2]_{aq,X}(T,P) \quad (5)$$

The density of brines, ρ_{brine}, is only slightly temperature-dependent, can be well approximated by an incompressible fluid and, for higher concentrations, generally increases[25] with decreasing temperatures by less than 5–10% from 298 K to 140 K. Therefore, by assuming that $\rho_{brine}(T,P) \approx \rho_w(T_{ref}, P_{ref}) \approx 1{,}000\,kg\,m^{-3}$, where ρ_w is the density of water, we attain an approximate lower estimate for the solubility of O_2.

Together, equations (1–5) allow us to calculate the solubility of O_2 in a variety of brines, across a wide range of temperatures, including those far below the freezing point of pure water, with the specific heat of dissolved O_2 as the major modulating factor.

Specific heats and robustness of conclusions. The specific heat at constant pressure of O_2 in the gas phase is experimentally well known down to 100 K, and remains approximately constant[44] at 300–100 K, with $C_{P,O_2,g}(T) \approx 29.332\,J\,K^{-1}\,mol^{-1}$, due to translational and rotational degrees of freedom remaining active throughout this temperature range.

The major factor impacting the solubility of O_2 in pure water is the heat capacity of dissolved O_2 as a function of temperature, $C_{P,O_2,aq}(T)$. Larger values of $C_{P,O_2,aq}(T)$ lead to a greater gas solubility. For temperatures of 273–373 K, experiments[32,40] show that $C_{P,O_2,aq}(T)$ increases approximately linearly with decreasing temperature towards 273 K; there are no data below 273 K for $C_{P,O_2,aq}(T)$. As we demonstrate later, there is good evidence that a trend of increasing heat capacity persists until at least ~225–235 K, where water might have a liquid–liquid phase transition[25], possibly leading to a decay of the specific heat of dissolved O_2 for lower temperatures.

Because of this uncertainty, we take a more conservative approach by considering (1) a best estimate with $C_{P,O_2,aq}(T) = C_{P,O_2,aq}(T = 298\ K)$, (2) reasonable alternatives for the specific heat capacity as a function of temperature, based on either the specific heat for supercooled water or a linear decay towards 140 K (similar to the specific heat of various brines[25,26])—leading to results of only less than a factor of ~3 smaller at 140 K than what we found with our best estimate, demonstrating the order-of-magnitude robustness of our conclusions with our best estimate, and (3) a conservative worst-case limit to the solubility of O_2 in water (see below, and in more detail in the Supplementary Information), as shown in Fig. 1c and Supplementary Fig. 1. The worst-case limit would lead, at 140 K, to a solubility about four orders of magnitude smaller than what we find with our best estimate. Although this worst case would limit high-O_2 oases with concentrations above the breathing limit for sponges[21], it would still permit O_2 solubilities up to 1–2 orders of magnitude above the aerobic limit for microorganisms[19,20] for modern Mars conditions.

Thermodynamic limit and worst-case scenario. $C_{P,O_2,aq}$ controls the solubility of O_2 in pure water or brine in the following manner (using equations (1–3); see Supplementary Sections 2.1.1 and 2.1.2 for details):

$$\begin{aligned}[O_2]_{aq}(T,\zeta) &= F(T)\exp\left(\frac{\zeta(T)}{RT}\right) \text{with } \zeta(T) \\ &= -\int_{T_{ref}}^{T} C_P(T')\,dT' + T\int_{T_{ref}}^{T} \frac{C_P(T')}{T'}\,dT'\end{aligned} \quad (6)$$

$F(T)$, defined as the solubility of O_2 if the specific heat of dissolved O_2 in water were always zero, is well constrained, and monotonically increases for lower temperatures. The function $\zeta(T)$, defined in equation 6, contains all the uncertainties introduced by the behaviour of $C_{P,O_2,aq}(T)$. We demonstrate in the Supplementary Information that $\zeta(T)$ also monotonically increases with decreasing temperatures, due to the specific heat always being larger than zero for $T > 0$ K.

Therefore, the minimum solubility of O_2 in pure water at $T < 273$ K is given by

$$[O_2]_{aq}(T)|_{min} = [O_2]_{aq}(T, \zeta^*), \text{ with } \zeta^*(T) = \zeta(T = 273\ K) \quad (7)$$

where the factor $\zeta(T)$ from equation 6 is set to a constant value, given by the lowermost temperature where $C_{P,O_2,aq}(T)$ is exactly known from experiments, which we set at 273 K. Our worst case provides the logic for a conservative lowermost bound on O_2 solubility, and it is important to note that the true solution is probably much greater and closer to our best-estimate scenario. This is because our worst-case solution indirectly implies that $C_{P,O_2,aq}(T) = 0$ for all $T < 273$ K, but thermodynamics teaches us that this limit can occur only at $T = 0$ K. Moreover, reasonable assumptions on $C_{P,O_2,aq}(T)$ below 273 K, as shown in 'Specific heats and robustness of conclusions', would lead to solubilities very close to our best estimate.

Melting curve for brines. Values for the critical concentration at T needed to keep the brine liquid, $m_X(T)$, are taken from experimental data[16,26,45] and fitted with a third-degree polynomial to generate a melting curve for the brine. Inside the

temperature domain where the brine is known to effectively supercool (between eutectic temperature, T_{eu}, and maximum supercooling temperature, T_{sc}; see Fig. 1a), we assume a eutectic concentration of $m_{eu} = m_X(T_{eu})$, as no additional salt has to be added to keep the brine liquid.

Therefore, we obtain $m_X(T) = \sum_{i=0}^{3} p_i T^i$ for a temperature $T > T_{eu}$ and $m_X(T) = m_{eu} = m_X(T_{eu})$ for $T \leq T_{eu}$ (the parameters T_{eu}, T_{sc}, m_{eu} and p_i can be found in Supplementary Table 3 in the Supplementary Information). The eutectic temperature is not a strong function of pressure, and the pressures on Mars support the liquid state of Mg- and Ca-perchlorate brines for limited and possibly extended periods (see Supplementary Section 2.1.5 for a discussion of brine existence under current Mars conditions).

GCM for Mars. We use the Mars Weather Research and Forecasting (MarsWRF)[24] GCM for this investigation. MarsWRF is a Mars-specific implementation of the PlanetWRF GCM[23]—a global model derived from the terrestrial mesoscale weather research and forecasting model[46]. MarsWRF solves the primitive equations by using a finite-difference methodology on an Arakawa C-grid[47]. Both the horizontal and vertical resolution of the model are variable and selectable at run time; we use a 40-layer vertical grid (0–80 km), following a modified-sigma (terrain-following) coordinate. The lowest model layer with this vertical grid is ~75–100 m above ground level, depending on location and season. We use a horizontal resolution of 5°×5°, which corresponds to a grid of 72 points in longitude×36 points in latitude. The total present-day atmospheric CO_2 budget, as well as the CO_2 ice albedo and emissivity for each hemisphere, are adjusted, a priori, until the modelled pressure curves best match those observed at the Viking lander 1 and 2 sites[48]. Both surface albedo and thermal inertia are matched to Mars Global Surveyor Thermal Emission Spectrometer observations[49,50], while water ice albedo and emissivity are fixed at 0.45 and 1.0, respectively.

The model includes a basic water cycle, which allows the condensation, sublimation, sedimentation and transport of water ice particles in the atmosphere, and growth and recession of polar water ice caps. Surface albedo is modified to the above-mentioned values when either CO_2 or water ice is condensed on the surface.

Planetary obliquity, or axial tilt, can be modified at run time in MarsWRF (ref. [51]). In all obliquity simulations, we hold other model parameters constant. To examine the past 20 Myr of Mars history, we assume the luminosity of the Sun to be at the present-day value. Because the frost-point temperature for CO_2 (~148 K at present surface pressure) is regularly reached in the polar winter hemisphere, the present-day Martian atmosphere cycles ~25% of its total mass over the course of the year into and out of the polar caps. For obliquities higher than the present-day value (~25°), this fraction is larger.

For runs with obliquity of 10°, we find that solar heating of the polar regions is insufficient to stave off condensation year-round, and Mars experiences episodes of atmospheric collapse, where the condensable species in the atmosphere (predominantly CO_2) form thick ice caps at the poles. We do not find such atmospheric collapse for an obliquity of 15° with our GCM runs. We assume, on the basis of our GCM results, that atmospheric collapse is likely to occur for obliquities below 10–15°. We indicate these intervals by the grey shading in Fig. 4, and, if theoretical predictions of obliquity as a function of time are correct, these events are uncommon in the period that we examine[22]. For this reason, then, we do not thoroughly explore this period in our study (although we discuss potential oxidation events at such phases in Supplementary Section 2.2.5.2.2).

At higher obliquities, water ice preferentially condenses at lower latitudes. While there is disagreement over exactly how widespread such water deposits might be[51,52], MarsWRF handles the tropical ice deposits self-consistently, increasing surface albedo at locations where ice is deposited. With all else equal, Mars at high obliquity will have a slightly lower global surface temperature than at present values, due to the increased surface area in the tropics covered by high albedo ice, as compared with the relatively small polar area covered by ice at present. However, the maximum (minimum) values of annually averaged surface temperature will generally decrease (increase) with increasing obliquity—mainly due to the albedo changes associated with obliquity change, as mentioned before. The distribution, minimum, average and maximum values of annually averaged surface temperature can be found in Supplementary Table 4. Obliquity variation with time is the major driver for differences in annual averages for surface temperature and pressure; past variations in eccentricity played only a minor role in annually averaged surface temperatures and pressures.

On Mars today, observations reveal a perennial polar cap of CO_2 ice in the south that requires the surface temperature to be set to the pressure-dependent CO_2 frost point for all latitudes poleward of −85° in the GCM. To examine how O_2 solubility changes with Mars's climate at different non-modern-day obliquities, we do not presume the presence of a residual CO_2 ice cap, because the mechanisms for forming it at present are not well understood. Consult Supplementary Section 2.2.2 for details of how the choice of a perennial polar cap of CO_2 ice in the south impacts our results.

The model water cycle mentioned above introduces water vapour into the atmosphere via sublimation of surface ice deposits, at a rate that is dependent on the temperature of those deposits. For the present day, the source of atmospheric vapour is the north polar cap, and the atmosphere contains a few to a few tens of precipitable micrometres of water vapour, depending on location and season. When a particular model grid point is saturated with water vapour, excess vapour is condensed as water ice and deposited on the surface. Water vapour is radiatively active and may influence atmospheric temperatures, although at the small abundances seen at most of the obliquities studied, it is a negligible effect. The water ice that is formed is not treated as radiatively active. This is an imprecise approach that can affect surface temperatures in certain locations (particularly in the polar hood regions and aphelion cloud belt) by a small amount. For this study, however, and with our lack of knowledge of cloud distribution and of the water cycle at other obliquities, it would be a speculative exercise to impose such behaviour—no better or worse than our current approach.

We do not include dust in the model atmosphere. This is done for the sake of consistency across obliquities and helps to expose the 'raw' trend of surface temperature over obliquity without the confounding effects of seasonally and interannually variable dust in the atmosphere. There is some suggestion that at high obliquity, there is greater dust loading in the Martian atmosphere[53]. However, the thermal impact of dust would not affect our overall results, which vary by orders of magnitude across the Martian near surface and with obliquity.

Code availability. The climate and solubility codes used for this study can be made available upon request from the authors.

Data availability

The generated data output from the climate model used for this study can be made available upon request from the authors.

References

40. Tromans, D. Temperature and pressure dependent solubility of oxygen in water: a thermodynamic analysis. *Hydrometallurgy* **48**, 327–342 (1998).
41. Tromans, D. Oxygen solubility modeling in inorganic solutions: concentration, temperature and pressure effects. *Hydrometallurgy* **50**, 279–296 (1998).
42. Toner, J. D., Catling, D. C. & Light, B. A revised Pitzer model for low-temperature soluble salt assemblages at the Phoenix site, Mars. *Geochim. Cosmochim. Acta* **166**, 327–343 (2015).
43. Khomutov, N. E. & Konnik, E. I. Solubility of oxygen in aqueous electrolyte solutions. *Russ. J. Phys. Chem.* **48**, 359–362 (1974).
44. Manion, J. A. et al. *NIST Standard Reference Database 17* Version 7.0 Release 1.6.8 (National Institute of Standards and Technology, 2016).
45. Li, D. et al. Phase diagrams and thermochemical modeling of salt lake brine systems. II. NaCl+H_2O, KCl+H_2O, $MgCl_2$+H_2O and $CaCl_2$+H_2O systems. *Calphad* **53**, 78–89 (2016).
46. Skamarock, W. C. & Klemp, J. B. A time-split nonhydrostatic atmospheric model for weather research and forecasting applications. *J. Comput. Phys.* **227**, 3465–3485 (2008).
47. Arakawa, A. & Lamb, V. R. Computational design of the basic dynamical processes of the UCLA general circulation model. *Methods Comput. Phys.* **17**, 173–265 (1977).
48. Guo, X., Lawson, W. G., Richardson, M. I. & Toigo, A. Fitting the Viking lander surface pressure cycle with a Mars general circulation model. *J. Geophys. Res.* **114**, E07006 (2009).
49. Christensen, P. R. et al. Mars Global Surveyor Thermal Emission Spectrometer experiment: investigation description and surface science results. *J. Geophys. Res.* **106**, 23823–23871 (2001).
50. Putzig, N. & Mellon, M. Apparent thermal inertia and the surface heterogeneity of Mars. *Icarus* **191**, 68–94 (2007).
51. Mischna, M. A. On the orbital forcing of Martian water and CO_2 cycles: a general circulation model study with simplifi d volatile schemes. *J. Geophys. Res.* **108**, E65062 (2003).
52. Forget, F., Haberle, R. M., Montmessin, F., Levrard, B. & Head, J. W. Formation of glaciers on Mars by atmospheric precipitation at high obliquity. *Science* **311**, 368–371 (2006).
53. Haberle, R. M., Murphy, J. R. & Schaeffer, J. Orbital change experiments with a Mars general circulation model. *Icarus* **161**, 66–89 (2003).